COMPRESSIVE IMAGING OF COLOR IMAGES

Pradeep Nagesh and Baoxin Li

Dept. of Computer Science & Engineering
Arizona State University, Tempe, AZ 85287, USA

ABSTRACT

In this paper, we propose a novel c*ompressive imaging* framework for color images. We first introduce an imaging architecture based on combining the existing single-pixel *Compressive Sensing* (CS) camera with a Bayer color filter, thereby enabling acquisition of compressive color measurements. Then we propose a novel CS reconstruction algorithm that employs joint sparsity models in simultaneously recovering the R, G, B channels from the compressive measurements. Experiments simulating the imaging and reconstruction procedures demonstrate the feasibility of the proposed idea and the superior quality in reconstruction.

Index Terms— Compressive Sensing, Bayer Color Filter, Joint Sparsity Models, l^1-Minimization.

1. INTRODUCTION

Modern digital cameras acquire an image in the form of millions of "pixels" and subsequently use transform coders like a JPEG or JPEG-2000 to reduce the data-rate for transmission or storage. In recent years a new signal acquisition theory known as *Compressive Sensing* (CS) has emerged, which provides a method for acquiring and compressing data simultaneously. According to CS, only M (with $M << N$) non-adaptive linear measurements of a K-sparse signal of N samples contain sufficient information for perfect reconstruction using non-linear optimization methods, provided that some conditions are satisfied [1,2]. Formally, let $\boldsymbol{x} \in \mathbb{R}^{\mathrm{N}}$be a real-valued signal that has sparse representation in a basis $\boldsymbol{\Psi} \in \mathbb{R}^{\mathrm{N}\times\mathrm{N}}$ (assume orthonormal for convenience). Suppose that we have a sensing system $\boldsymbol{\Phi} \in \mathbb{R}^{\mathrm{M}\times\mathrm{N}}$, with $M < N$ such that $\boldsymbol{\Phi}$ and $\boldsymbol{\Psi}$ are incoherent, then from a measurement of $\boldsymbol{x}$ defined as,

$$\boldsymbol{y} = \boldsymbol{\Phi x},\ \boldsymbol{y} \in \mathbb{R}^{\mathrm{M}} \tag{1}$$

one can recover $\boldsymbol{x}$ from $\boldsymbol{y}$ as long as the number of measurements M is of the order of $O(K\log(N))$, where K is the sparsity of $\boldsymbol{x}$ in the basis $\boldsymbol{\Psi}$ (i.e, K is the number of non-zero values in $\boldsymbol{\theta}$, $\boldsymbol{\theta} = \boldsymbol{\Psi^T x}, \boldsymbol{\theta} \in \mathbb{R}^{\mathrm{N}}$). The reconstruction is based on l^1 optimization:

$$(l^1) \qquad \widehat{\boldsymbol{\theta}} = arg\ min\|\boldsymbol{\theta}\|_1 \quad s.t.\ \boldsymbol{y} = \boldsymbol{\Phi\Psi\theta} \tag{2}$$

In the case of color imaging, one naïve approach would be to measure and reconstruct the R,G and B planes separately. This approach nevertheless cannot adequately exploit strong correlation among the color channels. Considering this fact and the reality of the wide-spread use of the Bayer filter in color imaging, in this paper we first introduce an imaging architecture for the acquisition of compressive color measurements based on combining the "single-pixel camera" [3] with a Bayer color filter. Then we propose a novel CS reconstruction algorithm that employs joint sparsity models in simultaneously recovering the R, G, B channels from the compressive measurements. We design experiments to evaluate the performance of the proposed algorithm. The results show that our method is able to produce significant improvement in reconstruction, compared with the naïve approach of processing the R, G and G channels separately.

The remaining of the paper is organized as follows. Section 2 introduces the architecture for compressive color imaging based on the single-pixel camera of [3]. Section 3 presents the proposed reconstruction algorithm. Section 4 provides our experimental results. We conclude with discussion on future work in Section 5.

2. A CS COLOR CAMERA ARCHITECTURE

For clarity and completeness, we first briefly review the working principle of the CS-based single-pixel-camera of [3] (more details can be also found in [4,5]). Refer to Fig. 1, ignoring the rotating color filter for the moment. Lens 1 captures an image of the scene on the digital micro mirror (DMD) array. With the help of pseudo-random number generator (RNG), randomly selected mirrors of DMD are oriented in a direction towards lens 2 (a "1"), while the rest are oriented in a different direction (a "0"). The net-effect is that the photodiode captures the summation of the light photons. This process can be interpreted as obtaining m^{th} measurement $\mathbf{y}(m)$ of Eqn. (1) ($m = 1,2 \ldots M$), as an inner product between the random vector $\phi_m \in \mathbb{R}^N$ (RNG configuration of 1s and 0s) and actual image $\boldsymbol{x} \in \mathbb{R}^N$. Here ϕ_m can be considered as rows to form the random measurement matrix ($\boldsymbol{\Phi} = [\phi_1\ \phi_2 \ldots \phi_M]^T \in \mathbb{R}^{M\times N}$). By simple calibrations, $\boldsymbol{\Phi}$ can be changed to other random structures of like -1/+1 etc [5].

We now introduce a simple way of extending the above single-pixel camera with a virtual Bayer filter for compressive acquisition of a color image. The basic idea is illustrated in Fig. 1. Fig. 1(a) shows the mosaic structure of the Bayer filter. In Fig. 1(b), the mirrors and the rotating color filter (RCF) are synchronized to allow the acquisition of the R, G and B pixels with a pattern corresponding to that of the actual Bayer filter. The RNG further allows random measurements of the R,G and B planes and can be configured seperately. Note that the G mirrors are explicitly labeled as G1 and G2, and we capture two separate measurements for G plane. Specifically, referring to Fig. 1(b), we explain the steps to capture the R plane (G1, G2 and B are similar to this). First, the Rotation Control ensures that the red portion of RCF is positioned between lens 1 and the DMD array and that only the R mirrors operate, while G1, G2 and B mirrors are turned off. Second, the RNG randomly chooses some R mirrors to point towards lens 2 and the rest away from it (this is the vector $\phi_m \in \mathbb{R}^{N/4}$). After $M_R$repetitions we get, the measurement vector $\boldsymbol{y_R}$ as,

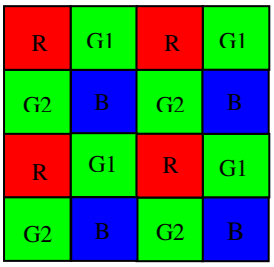

Fig 1(a)

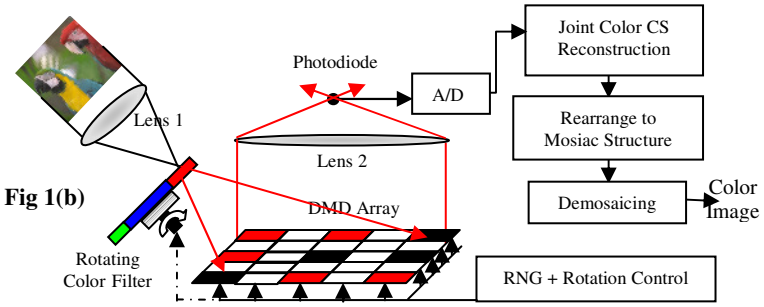

Fig 1(b)

Fig 1: (a) Shows "Virtual Bayer Filter" structure on the DMD array. There is no real Bayer filter, but each micro mirror is virtually "labeled" so that mosaic structure of a Bayer filter is formed. (b) Proposed color CS camera architecture. This has a Rotating Color Filter (RCF) and a Rotation Control unit (RC) as new components in the Camera of [3]. It captures R, G and B measurements directly on Bayer planes, (thereby reducing the overall measurements) and uses joint R-G-B reconstruction scheme to produce better quality color image.

$$\boldsymbol{y_R} = \boldsymbol{\Phi_R x_R}, \quad \boldsymbol{y_R} \in \mathbb{R}^{M_R \times 1} \tag{3}$$

where, $\boldsymbol{\Phi_R} = [\phi_1\ \phi_2 \dots \phi_M\ ]^T \in \mathbb{R}^{M_R \times N/4}$ is the random measurement matrix and $\boldsymbol{x_R}$ is sub-sampled image $\boldsymbol{x}$, with only samples retained from the alternate locations corresponding to the mosaic cell "R" of the Bayer filter. Mathematically we denote such a mapping function as $\boldsymbol{B_R}: \boldsymbol{x} \rightarrow \boldsymbol{x_R}$ or $\boldsymbol{x_R} = \boldsymbol{B_R(x)}$, with $\boldsymbol{x} \in \mathbb{R}^N$ and $\boldsymbol{x_R} \in \mathbb{R}^{N/4}$. We can define similar mapping functions $\boldsymbol{B_B}, \boldsymbol{B_{G1}}$ and $\boldsymbol{B_{G2}}$ for B, G_1 and G2 respectively. We call this "Bayer Measurement" and the process can be described by the following set of equations,

$$\left.\begin{aligned} \boldsymbol{y_R} &= \boldsymbol{\Phi_R B_R(x)}, & \boldsymbol{y_R} &\in \mathbb{R}^{M_R \times 1} \\ \boldsymbol{y_{G_1}} &= \boldsymbol{\Phi_{G_1} B_{G_1}(x)}, & \boldsymbol{y_{G_1}} &\in \mathbb{R}^{M_G \times 1} \\ \boldsymbol{y_{G_2}} &= \boldsymbol{\Phi_{G_2} B_{G_2}(x)}, & \boldsymbol{y_{G_2}} &\in \mathbb{R}^{M_G \times 1} \\ \boldsymbol{y_R} &= \boldsymbol{\Phi_B B_B(x)}, & \boldsymbol{y_B} &\in \mathbb{R}^{M_B \times 1} \end{aligned}\right\} \tag{4}$$

For color imaging, the Bayer filter compressive measurements are more efficient, since they reduce *(i)* the data-rate, exploiting the correlation between R-G-B pixels and *(ii)* acquisition time per color image. Note that this architecture is just a conceptual design and there may be more efficient ways of implementing a Bayer filter, depending on practical feasibility and costs. In addition, if the acquisition data rate or time is not a constraint, one could also obtain full R, G, B measurements using the RCF (i.e., forgoing the Bayer mosaic and capturing full R-G-B measurements). However, our main focus in this paper is to present an efficient color-image CS reconstruction scheme (Section 3), operating on reduced measurements captured with a Bayer filter, and thus we will assume that the data are acquired as discussed above.

3. PROPOSED RECONSTRUCTION ALGORITHM

With the compressive color measurements taken as discussed above, we now propose a CS approach for the reconstruction of the original color image, exploiting the inter-correlations among the R, G and B planes. The objective is to achieve better quality for the reconstructed images, compared to individually reconstructing the R, G, B images. To this end, we first present a baseline algorithm (Section 3.1) based on simple extension of the joint sparsity models (JSM) that has been proposed in the context of distributed compressive sensing of 1-D multi-sensor signals [6]. To fully utilize the specific inter-pixel relationship arising from the Bayer mosaic, in Section 3.2, we propose an extended JSM that aims at accounting for the spatial shift of the R, G, and B pixels.

3.1. Joint R-G-B Reconstruction: A Baseline Algorithm

Let $\boldsymbol{r}, \boldsymbol{g}$ and $\boldsymbol{b} \in \mathbb{R}^N$ be the raw R, G and B images, and $\boldsymbol{\theta_r}, \boldsymbol{\theta_g}$ and $\boldsymbol{\theta_b} \in \mathbb{R}^N$ be their transform coefficients (in a basis $\boldsymbol{\Psi}$). Similar to [6], we assume the following simple additive model,

$$\left.\begin{aligned} \boldsymbol{\theta_r} &= \boldsymbol{\theta^c} + \boldsymbol{\theta_r^i} = \boldsymbol{\Psi^T}(\boldsymbol{r^c} + \boldsymbol{r^i}) = \boldsymbol{\Psi^T r} \\ \boldsymbol{\theta_g} &= \boldsymbol{\theta^c} + \boldsymbol{\theta_g^i} = \boldsymbol{\Psi^T}(\boldsymbol{g^c} + \boldsymbol{g^i}) = \boldsymbol{\Psi^T g} \\ \boldsymbol{\theta_b} &= \boldsymbol{\theta^c} + \boldsymbol{\theta_b^i} = \boldsymbol{\Psi^T}(\boldsymbol{b^c} + \boldsymbol{b^i}) = \boldsymbol{\Psi^T b} \end{aligned}\right\} \tag{5}$$

where, $\boldsymbol{\theta^c} \in \mathbb{R}^N$ is a sparse component, common to $\boldsymbol{\theta_r}, \boldsymbol{\theta_g}$ and $\boldsymbol{\theta_b}$, derived from a common support $\boldsymbol{\Omega}$ (of non-zero coefficients), with cardinality K^c. Further, $\boldsymbol{\theta_r^i}, \boldsymbol{\theta_g^i}$ and $\boldsymbol{\theta_b^i}$ are the sparse innovation components that are unique to each image. If we let the sparsities of these components as $\|\boldsymbol{\theta_r^i}\|_0 = K_r^i$, $\|\boldsymbol{\theta_g^i}\|_0 = K_g^i$, $\|\boldsymbol{\theta_b^i}\|_0 = K_b^i$ and that of original images as, $\|\boldsymbol{\theta_r}\|_0 = K_r$, $\|\boldsymbol{\theta_g}\|_0 = K_g$, $\|\boldsymbol{\theta_b}\|_0 = K_b$, then, the joint representation of $\boldsymbol{r}, \boldsymbol{g}$ and $\boldsymbol{b}$, denoted as $\boldsymbol{S} = [\boldsymbol{\theta^c}\ \boldsymbol{\theta_r^i}\ \boldsymbol{\theta_g^i}\ \boldsymbol{\theta_b^i}]^T$ has sparsity $K = K^c + K_r^i + K_g^i + K_b^i$, while the independent representation has a total sparsity of $\widetilde{K} = K_r + K_g + K_b$. Since $\boldsymbol{r}, \boldsymbol{g}$ and $\boldsymbol{b}$ are sufficiently correlated, many coefficients in $\boldsymbol{\theta_r}, \boldsymbol{\theta_g}$ and $\boldsymbol{\theta_b}$ from support $\boldsymbol{\Omega}$ would be equal with high probability (or bounded within a small value ε in a practical case); hence "sparsity reduction" can be applied such that $K < \widetilde{K}$, as discussed in [6]. This is a process which involves extracting $\boldsymbol{\theta^c}$ from support $\boldsymbol{\Omega}$ such that the sum of sparsities of innovations $K_r^i + K_g^i + K_b^i$ is least. Note here that even $\boldsymbol{\theta^i}$'s can be intelligently chosen to help minimize $K_r^i + K_g^i + K_b^i$, if any two are equal. However, such a situation is taken care by the choice of $\boldsymbol{\theta^c}$. This joint representation, $\boldsymbol{S}$, with least possible sparsity is called "reduced sparsity representation" and can be recovered back by JSM reconstruction method as given below.

$$\widehat{\boldsymbol{S}} = arg\ min\ \|\boldsymbol{S}\|_1 \quad \boldsymbol{s.t.}\ \ \boldsymbol{y} = \widetilde{\boldsymbol{\Phi}}\widetilde{\boldsymbol{\Psi}}\boldsymbol{S} \tag{6}$$

where $\boldsymbol{y} = [\boldsymbol{y_r}\ \boldsymbol{y_g}\ \boldsymbol{y_b}]^T \in \mathbb{R}^{(M_r + M_g + M_b)}$ is a vector formed by individual $\boldsymbol{r}, \boldsymbol{g}$ and $\boldsymbol{b}$ measurements, $\widetilde{\boldsymbol{\Phi}} = \mathbf{diag}\left([\boldsymbol{\Phi_r}\ \boldsymbol{\Phi_g}\ \boldsymbol{\Phi_r}]^T\right)$ is a matrix whose diagonal elements are the individual measurement matrices $\boldsymbol{\Phi_r} \in \mathbb{R}^{M_r \times N}, \boldsymbol{\Phi_g} \in \mathbb{R}^{M_g \times N}$ and $\boldsymbol{\Phi_g} \in \mathbb{R}^{M_b \times N}$. Further, $\widetilde{\boldsymbol{\Psi}} = [\boldsymbol{A}\ \boldsymbol{B}]$, where $\boldsymbol{A} = [\boldsymbol{\Psi}\ \boldsymbol{\Psi}\ \boldsymbol{\Psi}]^T$ and $\boldsymbol{B} = \mathbf{diag}([\boldsymbol{\Psi}\ \boldsymbol{\Psi}\ \boldsymbol{\Psi}]^T)$. Owing to reduced sparsity of joint representation ($K < \widetilde{K}$), the R-G-B joint recovery is advantageous over the naïve approach since

(*i*) the minimum number of measurements required for faithful reconstruction is reduced; and (*ii*) conversely, for a fixed measurement (not sufficiently higher than $c\widetilde{K}$, $c \approx 4$), the fidelity of reconstructed image would be superior. This approach can also be extended for reconstructing the Bayer images from Bayer measurements, which is the reason why we split G plane into two separate G1 and G2 planes in Eqn. (4) so as to support an additive model similar to Eqn. (5). However, we may note that unlike the original $\boldsymbol{r}, \boldsymbol{g}$ and $\boldsymbol{b}$ images, the Bayer images $\boldsymbol{x_R}, \boldsymbol{x_{G1}}, \boldsymbol{x_{G2}}$ and $\boldsymbol{x_B}$ (from Bayer planes of Fig 1(a)) are not from aligned pixels positions, which means the inter-correlation is reduced, diminishing the efficacy of the baseline algorithm. This necessitates a better correlation model and recovery algorithm for reconstruction of Bayer images, which is presented next.

3.2. Extended Joint R-G-B Reconstruction (E-JSM)

Before we present the idea of E-JSM model, we would first like to discuss some key aspects of on Bayer images w.r.t JSM model. Under JSM of Eqn. (5) the "reduced sparsity representation" of the Bayer images ($\boldsymbol{x_R}, \boldsymbol{x_{G1}}, \boldsymbol{x_{G2}}$ and $\boldsymbol{x_B} \in \mathbb{R}^{N/4}$) can be written as,

$$\boldsymbol{S} = \left[\, \boldsymbol{\theta^c}\ \boldsymbol{\theta_R^i}\ \ \boldsymbol{\theta_{G_1}^i}\ \ \boldsymbol{\theta_{G_2}^i}\ \ \boldsymbol{\theta_B^i} \right]^T \in \mathbb{R}^{5N/4} \tag{8}$$

where, $\boldsymbol{\theta^c}$ is the common component extracted from a common support $\boldsymbol{\Omega_B}$ of cardinality K_B^c and $\boldsymbol{\theta^{i}}$*s* are innovation components. While this seems reasonable, noting that Bayer images exhibit reduced inter-correlation, we make the following observations,
(i) The common support $\boldsymbol{\Omega_B}$ of Bayer images is a smaller subset compared to $\boldsymbol{\Omega}$ of original image i.e., $4K_B^c/N \ \leq K^c/N$.
(ii) For the $\boldsymbol{r}, \boldsymbol{g}$ and $\boldsymbol{b}$ images, if we define the subset $\widetilde{\boldsymbol{\Omega}}$ ($\widetilde{\boldsymbol{\Omega}} \subset \boldsymbol{\Omega}$, cardinality $\widetilde{K}^c$) such that $\boldsymbol{\theta_r}(n) = \boldsymbol{\theta_g}(n) = \boldsymbol{\theta_b}(n)$ or $\boldsymbol{\theta_r}(n) \approx \boldsymbol{\theta_g}(n) \approx \boldsymbol{\theta_b}(n), \forall\, n \in \boldsymbol{\Omega}$ (or bounded within a small value $\boldsymbol{\varepsilon}$ for a practical case), and an equivalent version $\widetilde{\boldsymbol{\Omega}}_{\boldsymbol{BR}}$ for the Bayer images (cardinality $\widetilde{K}_{BR}^c$), we may write, $4\widetilde{K}_{BR}^c/N \ \leq \widetilde{K}^c/N$.

Observations (i) and (ii) suggest that, even after sparsity swapping, reduction in sparsity in the joint representation of Eqn.(8) is much smaller than the case of original $\boldsymbol{r}, \boldsymbol{g}$ and $\boldsymbol{b}$ images. However, since the Bayer R, G, B are neighboring pixels, they exhibit sufficient pair-wise correlation. So**,** in this sense, there is still redundancy in innovation components $\boldsymbol{\theta_R^i}$, $\boldsymbol{\theta_{G_1}^i}$, $\boldsymbol{\theta_{G_2}^i}$ and $\boldsymbol{\theta_B^i}$**,** say if we consider them, pair-wise. As an example, consider $\boldsymbol{\theta_R^i}$ and $\boldsymbol{\theta_{G_1}^i} \in \mathbb{R}^{N/4}$. For these two innovation images, we may still identify a common support of non-zero coefficients $\boldsymbol{\Omega}_{\mathrm{RG}_1}^i$ ($\left\|\boldsymbol{\Omega}_{\mathrm{RG}_1}^i\right\|_0 = K_{\mathrm{RG}_1}^i$) and its subset $\widetilde{\boldsymbol{\Omega}}_{\mathrm{RG}_1}^i$ ($\left\|\widetilde{\boldsymbol{\Omega}}_{\mathrm{RG}_1}^i\right\|_0 = \widetilde{K}_{\mathrm{RG}_1}^i$) such that $\boldsymbol{\theta_R^i}(n) = \boldsymbol{\theta_{G_1}^i}(n)$ (or $\boldsymbol{\theta_R^i}(n) \approx \boldsymbol{\theta_{G_1}^i}(n)$) $\forall\, n \in \widetilde{\boldsymbol{\Omega}}_{\mathrm{RG}_1}^i$. Thus, we can find a common component $\boldsymbol{\theta}_{RG1}^c$ by applying "pair-wise sparsity reduction" again, rather than letting the burden on the joint choice of $\boldsymbol{\theta^c}$ (and also corresponding $\boldsymbol{\theta^{i}}$'s of Eqn.(8)). We may now define a new E-JSM additive model considering a global common and all six pair-wise common components as follows,

$$\begin{aligned}
\boldsymbol{\theta_R} &= \boldsymbol{\theta^c} + \boldsymbol{\theta}_{\boldsymbol{RG_1}}^{\boldsymbol{c}} + \boldsymbol{\theta}_{\boldsymbol{RG_2}}^{\boldsymbol{i}} + \boldsymbol{\theta}_{\boldsymbol{RB}}^{\boldsymbol{c}} + \boldsymbol{\acute{\theta}_R^i} \\
\boldsymbol{\theta_{G_1}} &= \boldsymbol{\theta^c} + \boldsymbol{\theta}_{\boldsymbol{RG_1}}^{\boldsymbol{c}} + \boldsymbol{\theta}_{\boldsymbol{G_1G_2}}^{\boldsymbol{i}} + \boldsymbol{\theta}_{\boldsymbol{G_1B}}^{\boldsymbol{c}} + \boldsymbol{\acute{\theta}_{G_1}^i} \\
\boldsymbol{\theta_{G_2}} &= \boldsymbol{\theta^c} + \boldsymbol{\theta}_{\boldsymbol{RG_2}}^{\boldsymbol{c}} + \boldsymbol{\theta}_{\boldsymbol{G_1G_2}}^{\boldsymbol{i}} + \boldsymbol{\theta}_{\boldsymbol{G_2B}}^{\boldsymbol{c}} + \boldsymbol{\acute{\theta}_{G_2}^i} \\
\boldsymbol{\theta_B} &= \boldsymbol{\theta^c} + \boldsymbol{\theta}_{\boldsymbol{RB}}^{\boldsymbol{c}} + \boldsymbol{\theta}_{\boldsymbol{G_1B}}^{\boldsymbol{i}} + \boldsymbol{\theta}_{\boldsymbol{G_2B}}^{\boldsymbol{c}} + \boldsymbol{\acute{\theta}_B^i}
\end{aligned} \tag{9}$$

Under this mode we have a "sparser" joint representation as,

$$\boldsymbol{S_E} = \left[\, \boldsymbol{\theta^c}\ \boldsymbol{S_E^c}\ \boldsymbol{S_E^i} \right]^T \in \mathbb{R}^{11N/4} \tag{10}$$

where, $\boldsymbol{S_E^c} = [\boldsymbol{\theta}_{RG1}^{\boldsymbol{c}}\boldsymbol{\theta}_{RG2}^{\boldsymbol{c}}\ \boldsymbol{\theta}_{RB}^{\boldsymbol{c}}\ \boldsymbol{\theta}_{G1G2}^{\boldsymbol{c}}\ \boldsymbol{\theta}_{G1B}^{\boldsymbol{c}}\ \boldsymbol{\theta}_{G2B}^{\boldsymbol{c}}] \in \mathbb{R}^{6N/4}$ is the vector of pair-wise common components and $\boldsymbol{S_E^i} = \left[\, \boldsymbol{\acute{\theta}_R^i}\ \boldsymbol{\acute{\theta}_{G_1}^i}\ \boldsymbol{\acute{\theta}_{G_2}^i}\ \boldsymbol{\acute{\theta}_B^i} \right] \in \mathbb{R}^{4N/4}$ is a vector of new innovation components. The recovery of $\boldsymbol{S_E}$ given the measurements, $\boldsymbol{y_B} = \left[\boldsymbol{y_R}\, \boldsymbol{y_{G_1}} \boldsymbol{y_{G_2}}\, \boldsymbol{y_R}\right]^T$, is achieved by the following l^1 minimization,

$$\widehat{\boldsymbol{S}}_{\boldsymbol{E}} = arg\, min\, \|\boldsymbol{S_E}\|_1 \quad \boldsymbol{s.t}\ \ \boldsymbol{y_B} = \widetilde{\boldsymbol{\Phi}}_{\boldsymbol{B}}\widetilde{\boldsymbol{\Psi}}_{\boldsymbol{B}}\boldsymbol{S_E} \tag{11}$$

Here $\widetilde{\boldsymbol{\Psi}}$ matrix is given by $\widetilde{\boldsymbol{\Psi}}_{\boldsymbol{B}} = [\boldsymbol{A}\ \boldsymbol{B}\ \boldsymbol{C}] \in \mathbb{R}^{4N \times 11N/4}$, where $\boldsymbol{A} = [\boldsymbol{\Psi}\ \boldsymbol{\Psi}\ \boldsymbol{\Psi}\ \boldsymbol{\Psi}]^T$ corresponds to global common, $\boldsymbol{C} = \mathbf{diag}(\boldsymbol{A})$ for the innovation and the $\boldsymbol{B}$ matrix is a matrix whose columns have inverse basis $\boldsymbol{\Psi}$ at two locations corresponding to pair-wise common components and $\widetilde{\boldsymbol{\Phi}}_{\boldsymbol{B}} = \boldsymbol{diag}\left(\left[\boldsymbol{\Phi_R}\, \boldsymbol{\Phi_{G_1}}\, \boldsymbol{\Phi_{G_2}}\, \boldsymbol{\Phi_B}\right]^T\right)$**.** Having recovered $\widehat{\boldsymbol{S}}_{\boldsymbol{E}}$ as above, we can form the estimates of spatial Bayer images $\widehat{\boldsymbol{x}}_{\boldsymbol{R}}, \widehat{\boldsymbol{x}}_{\boldsymbol{G1}}, \widehat{\boldsymbol{x}}_{\boldsymbol{G2}}$ and $\widehat{\boldsymbol{x}}_{\boldsymbol{B}} \in \mathbb{R}^{N/4}$ using an inverse transform. The full $\boldsymbol{r}$, $\boldsymbol{g}$ and $\boldsymbol{b}$ images can then be obtained using any existing demosiacing techniques.

4. EXPERIMENTAL RESULTS

We designed experiments to simulate the imaging process as illustrated in Fig. 1 on MATLAB platform. The measurement matrices used were random sequences of -1/+1 (sampled from uniform distribution) and also real numbers in the range [-1, 1] with Gaussian distribution). We used the TV minimization algorithm [8] in reconstruction and performed all our experiments using 2D DCT basis. Given a high resolution color image, Bayer color filtering was simulated by taking the proper R, G1,G2 and B components. Then CS measurements through random matrices were obtained. We tested our approaches (both E-JSM and JSM) with various popular test images of different color and visual content, and compared the performances with the approach of independent CS reconstruction. Some sample test images are shown in the Fig. 2. The performance results (Table 1, overall PSNR) is evaluated for 30%, 25% Bayer measurements, with the reference image being a Bayer filtered and demosaiced (through bilinear interpolation) version of the raw test image. We note that both E-JSM and JSM outperform the independent reconstruction in all cases. The E-JSM outperformed JSM for most of the times (the only exception is for the Goldhill). Furthermore, visually and perceptually, the E-JSM approach was always found superior, with better preserved image details and fewer color artifacts. This is illustrated in Fig. 3 where in a cropped portion of some sample images are shown in full resolution for visual comparison.

5. CONCLUSION AND FUTURE WORK

We introduced a new scheme for color image acquisition by a CS camera, where we capture R, G and B measurements of alternate pixels according to Bayer mosaic filter structure. In the process the total measurements are reduced (Bayer measurements). Further, we introduced a new joint reconstruction scheme that works on the Bayer measurements and exploits the correlation between R, G and B to produce better quality for the reconstructed color image. Experiments demonstrated the advantage of the proposed method. We are working on further improving the approach by explicitly modeling the spatial shift of the R,G,B pixels in a Bayer mosaic.

6. REFERENCES

[1] E J. Candès and M B. Wakin "An Introduction to Compressive Sampling", *IEEE Signal Processing Magazine*, March 2008.

[2] D. L. Donoho, "Compressed sensing," *IEEE Trans. Inform. Theory*, vol. 52, pp. 1289–1306, July 2006.

[3] M.B. Wakin, J.N. Laska, M.F. Duarte, D. Baron, S. Sarvotham. D. Takhar K.F Kelly. R.G Baraniuk. "An Architecture for Compressive Imaging" *IEEE Image. Proc,* pp-1273-1276, Oct 2006.

[5] M. F. Duarte, M. A. Davenport, D. Takhar, J. N. Laska, T. Sun, K.F. Kelly, R.G. Baraniuk "Single Pixel Imaging Via Compressive Sensing" *IEEE Sig. Proc. Magazine, Spl. Issue on CS*, March 2008.

[4] D. Takhar, J. N. Laska, M. B. Wakin, M. F. Duarte, D. Baron, S. Sarvotham, K. F. Kelly, and R. G. Baraniuk, "A new compressive imaging camera architecture using optical-domain compression," in *Computational Imaging IV*, vol. 6065, (San Jose, CA), pp. 43–52, Jan. 2006.

[6] D. Baron, M. Wakin, M. Duarte, S. Sarvotham, and R. Baraniuk, "Distributed Compressed Sensing", Preprint, 2005, Available online at http://www.dsp.ece.rice.edu/cs/

[7] J. Romberg "Imaging via Compressive Sampling", *IEEE Sig. Proc Magazine, Special Issue on Compressive Sampling,* March 2008.

[8] E. Candes and J. Romberg, "Practical signal recovery from random projections," 2005, preprint. [Online]. Available: http://www.dsp.ece.rice.edu/cs/

Table 1: Performance results on sample images of Figure 2.

Name	**BM*** (%)	**EJSM** PSNR** (dB)	**JSM** PSNR** (dB)	**CS** PSNR** (dB)	Name	**BM*** (%)	**EJSM** PSNR** (dB)	**JSM** PSNR**(dB)	**CS** PSNR** (dB)
Lena	30	**30.034**	29.093	29.172	Lady	30	**27.613**	27.305	26.291
	25	**28.16**	26.777	28.15		25	**26.82**	26.551	25.631
Pepper	30	**29.714**	28.395	28.077	Gold Hill	30	29.689	**29.838**	27.838
	25	**28.027**	26.947	26.628		25	28.639	**28.891**	26.927
Light House	30	**26.991**	26.692	25.189	Girl	30	**28.821**	28.278	27.555
	25	**26.105**	25.732	24.200		25	**27.714**	27.080	26.405

***BM:** Bayer Measurements (section 2). An X% Bayer measurement means X/4% measurement data each on R & B planes, X/2% on G.
** **PSNR** here is measured between reconstructed image (CS/EJSM/JSM) and Bayer filtered, demosaiced (bilinear interploation) image.

Fig. 3: Shows image sections & corresponding results. Column-wise: Col 1 is the Bayer sampled and demoisaiced reference image (bilinear interpolation), Col 2,3 are joint R-G-B E-JSM, JSM reconstructed images respectively. Col 4 is R,G,B independently reconstructed images. Row-wise: cropped sections of original images, Lady, Light-House and Pepper in Rows 1,2 and 3 respectively.

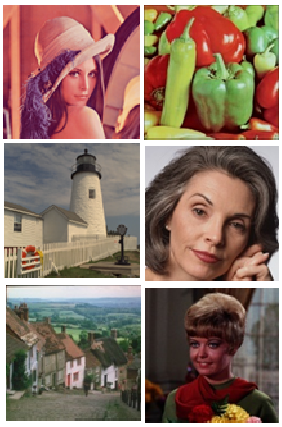

Fig. 2: Shows some sample high resolution color images used for testing. From top right, Lena, Peppers, Light-House, Lady, Gold-Hill and Girl. The performance results on these images are tabulated in Table 1, for 30%, 25% measurements on the Bayer R, G1, G2 and B planes.